Journal Title
XX(X):1–10

DOI: 10.1177/ToBeAssigned
www.sagepub.com/
SAGE

Dynamic model of a cylindrical roller on a rough surface, with applications to wind turbine gearbox planetary bearings

W James McBride[1] and Hugh EM Hunt[1]

Abstract

Wind turbines of larger power ratings have become increasingly prevalent in recent years, improving the viability of wind energy as a sustainable energy source. However, these large wind turbines have been subjected to higher rates of failure of the wind turbine gearbox, resulting in larger downtime of operation and an increase in cost due to repairs. These failures most frequently initiate in the gearbox's bearings, especially in the planetary bearings of the planetary stage and high-speed bearings. Currently, most of the research on the detection of planetary bearing faults only address the case of localised faults in the outer bearing race, while little research considers the detection of distributed bearing faults. The research that does consider distributed bearing faults relies on techniques – such as machine learning for the identification of faulty bearings – that do not account much for the underlying physics of the bearing. In this paper, a model is developed to simulate and analyse the dynamic interaction of a planetary bearing in the presence of surface roughness – which can be used to represent a distributed fault. The model presented uses random vibration theory for simulating the response of the planet bearing induced by distributed faults. The input of the model considers statistical expressions of the roughness geometry using multiple parallel tracks. Numerical simulation of the random vibration of the model is performed using 16 tracks, and the power spectral density of the radial deflection of the roller and the roller-race contact force is determined. The results of the simulation with the multi-track model show that a single-track model significantly overestimates the power spectral densities, and also suggests the stiffness of the bearing race is too high to have an effect on the roller dynamics for a planet bearing.

Keywords

Power spectral density, wind turbine gearbox, planetary bearings, cylindrical roller bearings, surface roughness

Introduction

Wind turbines have been increasing in power rating over recent years. However, failure of the gearbox – one of the most expensive components of the wind turbine – has in turn become prevalent. Based on around 350 off-shore wind turbines in Europe, the gearbox and generator alone account for 95% of failures that result in repairs excessive of 10,000 euros[1]. One of the most prevalent sources of failure in the gearbox are the planetary bearings, in which failures commonly take the form of distributed faults. The study of these faults themselves have been the subject of much research. Kotzalas and Doll[2] write that there are three main types of failure in wind turbine planet bearings, these being micropitting, smearing and white etching cracks. Ruellan et al.[3] and Evans[4] investigate further white etching cracks, noting these cracks are responsible for flaking of the material structure of the bearings. Both micropitting and white etching cracks influence the microstructure, and can be characterised as surface roughness.

The use of vibrational analysis to model roller bearings with distributed faults has been used by Sawalhi and Randall[5], who model the surface roughness as low-pass filtered Gaussian noise, and a cyclostationary analysis is performed to account for the roller entering and exiting distributed fault regions. This was then modified by Dolenc and Bokoski[6] to then account for variations in bearing roller diameters. Roller bearings with surface roughness were investigated by Takabi and Khonsari[7] with considerations to the lubrication schemes of roller bearings.

The modelling of the dynamics of a roller bearing with distributed faults may be considered as a cylinder rolling on a rough surface. This consideration allows research from other fields to be applied to this context. For instance, research has been performed in the dynamics of train wheels rolling over a corrugated rail, where Bogacz and Kowalska[8] consider a deterministic profile for the rail. The use of multiple tracks to determine the impact of roughness on rolling wheels has been applied to modelling the response of a car to road roughness[9]. However, no research has been found that applies this multi-track model to the dynamics of roller bearings. The length of cylindrical rollers are considerable to the extent that consideration of the surface roughness in two dimensions may have a significant impact. Therefore, this paper aims to model a roller bearing with a rough surface represented by a series of parallel rough tracks.

The novelty of this approach lies in the use of random vibration theory to simulate the vibrational behaviour of

[1]Department of Engineering, University of Cambridge, UK

Corresponding author:
W James McBride, Department of Engineering, University of Cambridge, Trumpington Street, Cambridge, Cambridgeshire, CB2 1PZ, UK.
Email: wjm36@cam.ac.uk

a planet bearing with distributed faults, and how this allows determination of a vibration response arising from a statistical geometric representation of the fault using purely physically reasoning. No research has been found that investigates the dynamics of random vibrations in cylindrical roller bearings in the presence of distributed faults considering the flexibility of the raceways and the contact stiffness. The power spectral density is a powerful approach that can be used to quantify the roughness of a distributed fault, and therefore it is desirable to be able to understand how the transmission of vibration induced from a fault to a sensor impacts the power spectral density. Furthermore, an analysis of the power spectral density of the contact forces that arise due to distributed faults will prove useful in estimation of the influence of the fault on fatigue life. While the type of bearing analysed in this paper has a fixed axis of rotation, the authors intend to extend the research to the case of planetary gearing, a type of gearing prevalently used in modern wind turbines, for the detection of faults of planet bearings in wind turbine gearboxes. The transmission path from the distributed fault of a planet bearing to an accelerometer on the ring gear is complicated and time-varying, and so an understanding of the dynamics and its effect on the fault-induced random vibration is desired: the model presented would provide the foundation for this approach.

The primary planetary bearing used in Nejad et al.[10] was used as a reference bearing for the variables used to perform the simulations. Table 1 summarises the variables associated with this reference bearing.

Bearing-roughness model

Figure 1 displays the dynamic model used in this paper. The model consists of three main elements:

1. The cylindrical bearing roller
2. The beam-foundation system
3. Several tracks of roughness

The beam-foundation system is used to model the dynamics of the bearing race, and consists of an Euler-Bernoulli beam – with bending stiffness EI and mass-per-unit-length m – resting on an elastic foundation with stiffness-per-unit-length k. $y(x,t)$ is the transverse deflection of the beam at a point x along its length. On the surface of the beam are several tracks of roughness, and the profile of each track $\varepsilon_j(x)$ is modelled as a random process, for $j = 1, 2 \dots N_\varepsilon$, where N_ε is the number of tracks used to represent the rough surface. At this stage, the curvature of the bearing race (as opposed to being straight like a beam) had been neglected. This was done initially for simplifying purposes. However, one way the results could be improved is by incorporating the radius of the race into an effective radius instead of using just the roller radius. That is,

$$\frac{1}{R_{ef}} = \frac{1}{R} + \frac{1}{R_{i/o}}. \tag{1}$$

where $R_{i/o}$ is the signed radius of the inner/outer race (negative for the concave outer race). In the future, the effect of curvature of the bearing race will be better incorporated into the model.

The stiffness-per-unit-length of the foundation is based on the results of Vesic[11]; the bearing outer race is contained within the bore of one of the planet gears. Assuming the planet gear is sufficiently solid, the race-bore interface can be likened to a beam on an elastic half-space.

In this model, the roller is constrained from motion in the horizontal direction, and the tracks of roughness are travelling at constant velocity V. The assumption that the velocity of the roller relative to the tracks of roughness is constant is suitable given that the amplitude of the roughness is sufficiently small to have a negligible influence of the horizontal motion of the roller. In the frame of reference adopted, the beam-foundation system would also be travelling at velocity V. However, for reasons that will be later justified in this paper, the beam-foundation system is stationary in the horizontal direction. Therefore, the model is analogous to a sheet of roughness being pulled out from between a roller and a beam-foundation system. The impact that rotation of the roller has is neglected in this model.

The contact between the roller and each track of roughness is modelled by connection of the roller to each track with a spring and damper. The spring stiffness is selected based on a linearisation of Hertzian contact theory, and the damper is selected to achieve a desired damping ratio of 0.01.

Dynamics of beam-foundation system

The undamped equation of motion governing the dynamics of an Euler-Bernoulli beam on a Winkler elastic foundation in response to a point force, of time-varying magnitude travel with constant velocity V, is

$$EIy'''' + m\ddot{y} + ky = -F(t)\delta(x - Vt). \tag{2}$$

The dot notation is used to represent $\partial/\partial t$, and the prime notation to represent $\partial/\partial x$. A positive value for F corresponds to a downward-pointing force. Many vibrating systems in reality have some degree of damping present. Rayleigh damping is incorporated into the beam-foundation system by making the following substitutions in frequency domain

$$\begin{aligned} m &\to m\left(1 - i\alpha_m/\omega\right) \\ E &\to E\left(1 + i\beta_E\omega\right) \\ k &\to k\left(1 + i\beta_k\omega\right), \end{aligned} \tag{3}$$

where α_m is the mass-proportional damping coefficient associated with the mass of the beam, and β_E and β_k are the stiffness-proportional damping coefficients, associated with the stiffness of the beam and the foundation respectively. The resulting equation of motion in time domain is

$$\begin{aligned} EI\left(y'''' + \beta_E\dot{y}''''\right) + m\left(\ddot{y} + \alpha_m\dot{y}\right) \\ + k\left(y + \beta_k\dot{y}\right) = -F(t)\delta(x - Vt). \end{aligned} \tag{4}$$

In order to be of use to the roller-roughness interaction model, a frame of reference following the point force would be adopted. However, if the velocity of the roller is considerably less than a critical velocity, then the velocity of the point force will have negligible impact. The value of the critical velocity is given by[12]

$$V_c = \sqrt{\frac{k}{m}}\left(\frac{4EI}{k}\right)^{1/4}. \tag{5}$$

Table 1. The parameters based on the reference bearing.

Variable	Value	Units	Description
M	5.5	kg	Mass of roller
K	2×10^{10}	$\mathrm{N\,m^{-1}}$	Contact stiffness
C	6.6×10^{3}	$\mathrm{N\,m^{-1}\,s}$	Contact damping
V	0.25	$\mathrm{m\,s^{-1}}$	Roller velocity
R	3×10^{-2}	m	Roller radius
B	250	mm	Length of roller
m	40	$\mathrm{kg\,m^{-1}}$	Beam mass per unit length
EI	3500	$\mathrm{N\,m^{2}}$	Beam bending stiffness
k	3.5×10^{11}	$\mathrm{N\,m^{-2}}$	Foundation stiffness per unit length
α_m	1×10^{3}	$\mathrm{s^{-1}}$	Mass-proportional damping in beam
β_E	1×10^{-7}	s	Stiffness-proportional damping in beam
β_k	1×10^{-7}	s	Stiffness-proportional damping in foundation

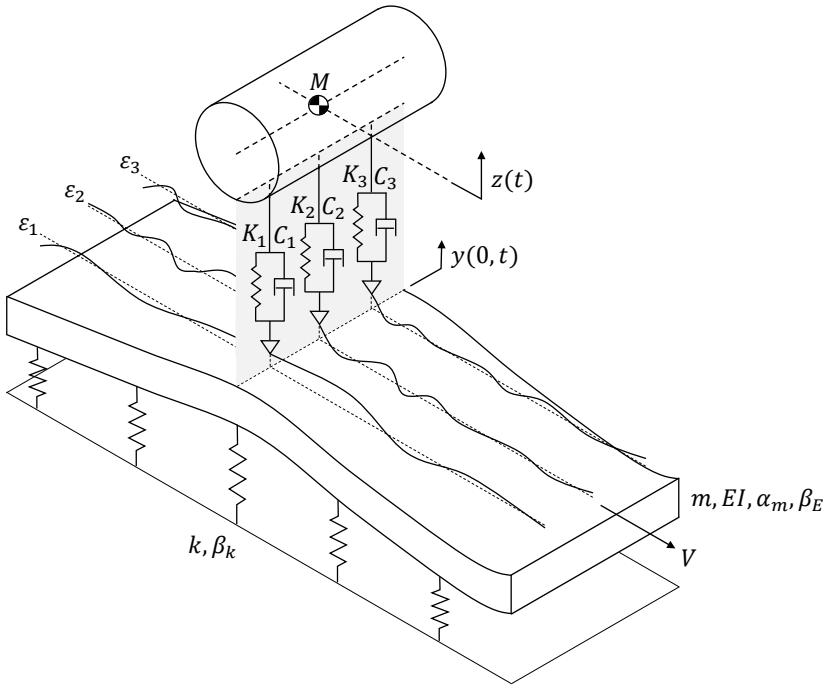

Figure 1. The roller-roughness interaction model, consisting of a beam-foundation system, a number of tracks of roughness, and a cylindrical roller.

For the reference planetary bearing, the critical velocity is around $1320\,\mathrm{m\,s^{-1}}$, whereas the roller velocity V is only $0.25\,\mathrm{m\,s^{-1}}$, and so the impact of velocity on the beam-elastic system can be neglected. Therefore, the following equation is sufficient in describing the dynamics of the beam-foundation system in the model,

$$EI\left(y'''' + \beta_E \dot{y}''''\right) + m\left(\ddot{y} + \alpha_m \dot{y}\right) + k\left(y + \beta_k \dot{y}\right) = -F(t)\delta(x). \quad (6)$$

Equation of motion of the model

With reference to Figure 1, the compressive contact force that the roller and bearing race mutually exert is given by

$$F(t) = \sum_{j}^{N_\varepsilon} \left\{ C_j \left(\dot{y}(0,t) + \dot{\varepsilon}_j - \dot{z} \right) + K_j \left(y(0,t) + \varepsilon_j - z \right) \right\}, \quad (7)$$

where K_j and C_j are the contact stiffness and damping between the roller and the jth track, and ε_j is the roughness of the jth track. Therefore, the equation of motion governing the roller is

$$M\ddot{z} + C_\Sigma \dot{z} + K_\Sigma z = C_\Sigma \dot{y}(0,t) + K_\Sigma y(0,t) + \sum_{j}^{N_\varepsilon} \left(C_j \dot{\varepsilon}_j + K_j \varepsilon_j \right), \quad (8)$$

where M is the roller mass, $K_\Sigma = \sum_j^{N_\varepsilon} K_j$, and $C_\Sigma = \sum_j^{N_\varepsilon} C_j$. Therefore, from (7) and (8), the contact force can be re-expressed more compactly as

$$F(t) = M\ddot{z}, \tag{9}$$

and so the equation of motion governing the beam-foundation system becomes

$$EI\left(y'''' + \beta_E \dot{y}''''\right) + m\left(\ddot{y} + \alpha_m \dot{y}\right) + k\left(y + \beta_k \dot{y}\right) = -M\ddot{z}(t)\delta(x). \tag{10}$$

Equations (8) and (10) are sufficient in governing the dynamic behaviour of the system.

Frequency response functions

In order to perform random vibration analysis, the frequency response function for the output $z(t)$ in response to each input $\varepsilon_j(t)$ for $j = 1, 2 \ldots N_\varepsilon$ needs to be determined. This is defined as

$$H_{z\varepsilon_j}(\omega) = \frac{\hat{z}(\omega)}{\hat{\varepsilon}_j(\omega)}, \tag{11}$$

where the $\hat{}$ notation refers to the Fourier transform of the variable, and ω is the frequency, in radians per unit time. It is also convenient to define a frequency response function of $y(x,t)$ in response to $z(t)$,

$$H_{yz}(x,\omega) = \frac{\hat{y}(x,\omega)}{\hat{x}(\omega)}. \tag{12}$$

Performing the (temporal) Fourier transform on both sides of Equation (10) yields

$$\left\{EI\left(1 + \mathrm{i}\beta_E\omega\right)\frac{\partial^4}{\partial x^4} + m\left(-\omega^2 + \mathrm{i}\alpha_m\omega\right) + k\left(1 + \mathrm{i}\beta_k\omega\right)\right\}\hat{y}(x,\omega) = M\omega^2\hat{z}(\omega)\delta(x), \tag{13}$$

and so an equation for $H_{yz}(x,\omega)$ is obtained:

$$\left\{EI\left(1 + \mathrm{i}\beta_E\omega\right)\frac{\partial^4}{\partial x^4} + m\left(-\omega^2 + \mathrm{i}\alpha_m\omega\right) + k\left(1 + \mathrm{i}\beta_k\omega\right)\right\}H_{yz}(x,\omega) = M\omega^2\delta(x), \tag{14}$$

To determine $H_{yz}(x,\omega)$ involves having to solve a differential equation. Alternatively, the spatial Fourier transform can be performed to yield

$$\hat{H}_{yz}(\gamma,\omega) = \frac{M\omega^2}{2\pi}\left\{EI\left(1 + \mathrm{i}\beta_E\omega\right)\gamma^4 + m\left(-\omega^2 + \mathrm{i}\alpha_m\omega\right) + k\left(1 + \mathrm{i}\beta_k\omega\right)\right\}^{-1}, \tag{15}$$

where γ is the wavenumber, in radians per unit length. Now it is possible to obtain values for $\hat{H}_{yz}(\gamma,\omega)$ over the desired range of γ and ω, from which $H_{yz}(x,\omega)$ can be obtained by performing the spatial inverse Fourier transform.

Considering the response from only track j, taking the Fourier transform of Equation (8) gives

$$\left(-M\omega^2 + \mathrm{i}C_\Sigma\omega + K_\Sigma\right)\hat{z}(\omega) = \left(\mathrm{i}C_\Sigma\omega + K_\Sigma\right)\hat{y}(0,\omega) + \left(\mathrm{i}C_j\omega + K_j\right)\hat{\varepsilon}(\omega), \tag{16}$$

and so the frequency response functions can be expressed as

$$H_{z\varepsilon_j}(\omega) = \frac{\mathrm{i}C_j\omega + K_j}{\left(-M\omega^2 + \mathrm{i}C_\Sigma\omega + K_\Sigma\right) - \left(\mathrm{i}C_\Sigma\omega + K_\Sigma\right)H_{yz}(0,\omega)}. \tag{17}$$

It is also useful to obtain an expression for the frequency response of the contact force $H_{F\varepsilon_j}$, which – from equation (9) – can be shown to be

$$H_{F\varepsilon_j}(\omega) = \frac{-M\omega^2\left(\mathrm{i}C_j\omega + K_j\right)}{\left(-M\omega^2 + \mathrm{i}C_\Sigma\omega + K_\Sigma\right) - \left(\mathrm{i}C_\Sigma\omega + K_\Sigma\right)H_{yz}(0,\omega)}. \tag{18}$$

In this paper, the contact stiffness and damping are taken to be uniform across the lines of contact, so $C_j = C = C_\Sigma/N_\varepsilon$ and $K_j = K = K_\Sigma/N_\varepsilon$, and so each frequency response function become equal to the transfer function for a single-track case divided by the number of tracks.

For the parameters provided in Table 1, the frequency response functions are obtained for both $z(t)$ and $F(t)$, and shown in Figures 2 and 3 respectively. For each, two curves have been plotted: the solid lines represent the frequency response for the model as described above. The dashed lines represent the frequency response for the model excluding the effect that the deflection of the beam has, i.e. $EI, k \to \infty$. Note the resulting shift in resonant frequency due to the beam-foundation element of the model: the peak shifts from $6000\,\mathrm{rad\,s^{-1}}$ to $3950\,\mathrm{rad\,s^{-1}}$.

Transmission of random vibrations

The theory of random vibrations is applied to the model in order to determine the statistics of the response of the bearing system to the surface roughness without unnecessarily narrowing down to the case of a single instance of a random surface. This subject is covered extensively by Newland [13]. It can be shown that the power spectral densities of the outputs $z(t)$ and $F(t)$ are related to those of the inputs $\varepsilon_j(t)$ by the following equations [13]:

$$S_{zz}(\omega) = \sum_{j=1}^{N_\varepsilon}\sum_{k=1}^{N_\varepsilon} H^*_{z\varepsilon_j}(\omega)H_{z\varepsilon_k}(\omega)S_{\varepsilon_j\varepsilon_k}(\omega), \tag{19}$$

$$S_{FF}(\omega) = \sum_{j=1}^{N_\varepsilon}\sum_{k=1}^{N_\varepsilon} H^*_{F\varepsilon_j}(\omega)H_{F\varepsilon_k}(\omega)S_{\varepsilon_j\varepsilon_k}(\omega), \tag{20}$$

where * represents the complex conjugate operator. $S_{ff}(\omega)$ is the power spectral density of a signal $f(t)$, and $S_{fg}(\omega)$ is the cross spectral density between signals $f(t)$ and $g(t)$.

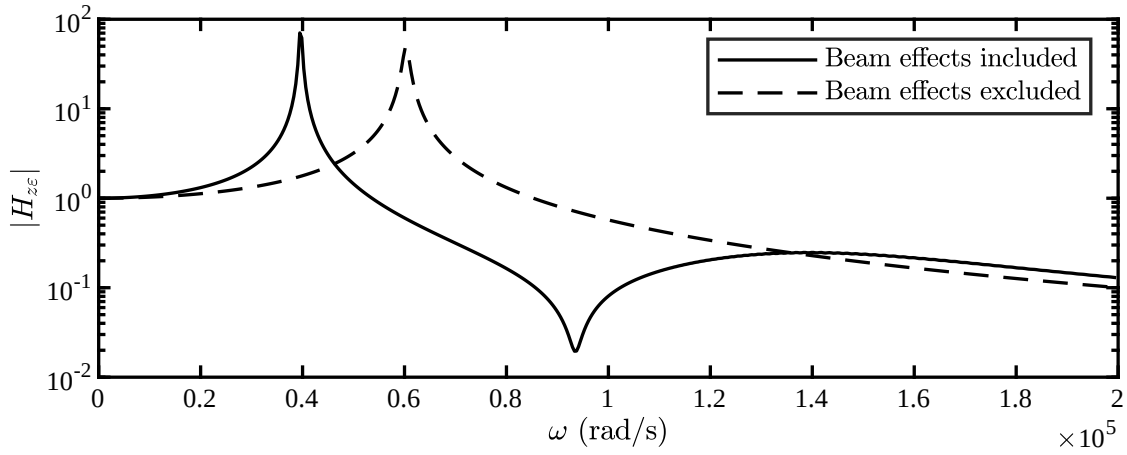

Figure 2. The absolute value of the frequency response function of the roller height in response to the surface roughness, using the parameters listed in Table 1. For $N_\varepsilon = 1$.

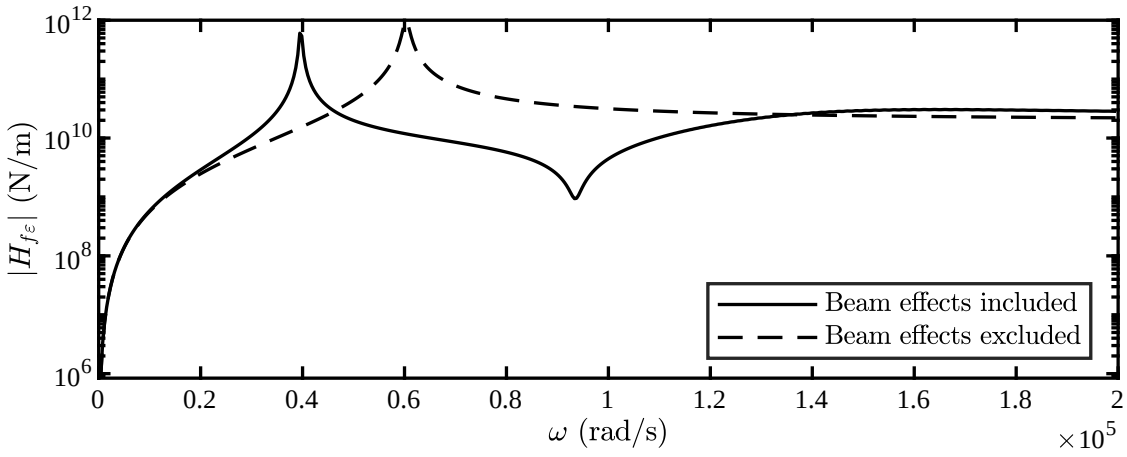

Figure 3. The absolute value of the frequency response function of the roller-race contact force in response to the surface roughness, using the parameters listed in Table 1. For $N_\varepsilon = 1$.

Modelling of a single track of roughness

Each track is modelled as a random process, and – in order to perform a random vibration analysis – is defined by its power spectral density.

For any random signal in time $x(t)$, its autocorrelation function is defined as [13]

$$R_{xx}(t,\tau) = \mathrm{E}[x(t)x(t+\tau)], \tag{21}$$

where $\mathrm{E}[\cdot]$ is the average over the ensemble of possible instances of the random signal. It is assumed that all random processes considered in the model are stationary; that is, the auto-correlation functions are independent of absolute time t: $R_{xx}(t,\tau) = R_{xx}(\tau)$. From this, the power spectral density is defined as the Fourier transform of the autocorrelation function: [13]

$$S_{xx}(\omega) = \frac{1}{2\pi}\int_{-\infty}^{\infty} R_{xx}(\tau)\mathrm{e}^{-\mathrm{i}\omega\tau}\,\mathrm{d}\tau. \tag{22}$$

These definitions also extend to spatial signals. At this stage, a highly simplified model for the surface roughness is used; this is chosen to be white noise with a sharp cut-off wavenumber. For a single track $\varepsilon(x)$, this is defined as

$$S_{\varepsilon\varepsilon}(\gamma) = \begin{cases} S_0 & \text{for } |\gamma| \le \gamma_{\max} \\ 0 & \text{otherwise.} \end{cases} \tag{23}$$

A cut-off frequency is specified as, above a certain wavenumber, the curvature of the roughness κ_ε begins to exceed that of the roller $1/R$, and so the roller can only physically make contact with the asperities of the roughness, which is unaccounted for by the current model. Therefore, the value of $\gamma_{\max}$ is selected so that the curvature of the roughness does not exceed the roller roughness for a sufficiently high proportion of the roughness. If the curvature of the roughness is assumed to be a random process with a Gaussian distribution, it is possible to ensure that the roughness curvature remains below $1/R$ for around 99.73% of the roughness length. That is, the standard deviation of the curvature σ_κ and the roller radius are related by

$$3\sigma_\kappa = \frac{1}{R}. \tag{24}$$

An exact expression for the curvature of $\varepsilon(x)$ is

$$\kappa_\varepsilon = \frac{\varepsilon''}{\left(1+(\varepsilon')^2\right)^{3/2}}. \tag{25}$$

However, by assuming that ε' is small – which is indeed the case for a surface whose curvature and amplitude is less than that of the roller – the curvature can be approximated by the linear expression

$$\kappa_\varepsilon = \varepsilon''. \tag{26}$$

Therefore it is possible to obtain the spectral density for the curvature. The relationship between the power spectral densities of $\varepsilon(x)$ and its derivatives is given as [13]

$$S_{\varepsilon'\varepsilon'} = \gamma^2 S_{\varepsilon\varepsilon}, \qquad S_{\varepsilon''\varepsilon''} = \gamma^4 S_{\varepsilon\varepsilon}. \tag{27}$$

Then the standard deviation of the curvature can be calculated with

$$\sigma^2_{\varepsilon''} = E\left[(\varepsilon'')^2\right] = R_{\varepsilon''\varepsilon''}(0) = \int_{-\infty}^{\infty} S_{\varepsilon''\varepsilon''}(\gamma)\,\mathrm{d}\gamma \tag{28}$$

Then by substituting the expression for $S_{\varepsilon\varepsilon}(\gamma)$ into (27),

$$\sigma^2_{\varepsilon''} = \int_{-\gamma_{\max}}^{\gamma_{\max}} S_0\gamma^4\,\mathrm{d}\gamma = \frac{2}{5}S_0\gamma_{\max}^5. \tag{29}$$

From (24),

$$18R^2S_0\gamma_{\max}^5 = 5. \tag{30}$$

The value of S_0 can be related to σ_ε,the standard deviation of $\varepsilon(x)$, by noting that the area under $S_{\varepsilon\varepsilon}(\gamma)$ is equal to σ^2_ε, and so,

$$S_0 = \frac{\sigma^2_\varepsilon}{2\gamma_{\max}}. \tag{31}$$

Now values for $\gamma_{\max}$ and S_0 can be obtained in terms of R and σ_ε:

$$\gamma_{\max} = \sqrt{\frac{\sqrt{5}}{3R\sigma_\varepsilon}} \approx 0.8633\frac{1}{\sqrt{R\sigma_\varepsilon}}, \tag{32}$$

$$S_0 = \sqrt{\frac{3R\sigma^5_\varepsilon}{4\sqrt{5}}} \approx 0.5791\sqrt{R\sigma^5_\varepsilon}. \tag{33}$$

Now that the spatial spectral density for the surface roughness $S_{\varepsilon\varepsilon}(\gamma)$ is determined, the temporal spectral density $S_{\varepsilon\varepsilon}(\omega)$ can be determined with [13]

$$S_{\varepsilon\varepsilon}(\omega) = \frac{1}{V}S_{\varepsilon\varepsilon}\left(\gamma = \frac{\omega}{V}\right). \tag{34}$$

Modelling of multiple tracks of roughness

Because the roller is a three-dimensional cylinder that makes contact with the bearing race over a finite length, using a single track of roughness may not be sufficiently representative of the roughness of the race surface. For this reason, finitely many parallel tracks are included. Note that the roughness for each track $\varepsilon_j(x)$ is correlated to one another, and we should expect this correlation to increase for tracks of lower separation, becoming perfectly correlated as the separation tends toward zero. It is therefore necessary to determine the cross spectral density between the tracks, and this can be done by determining the power spectral density of the two-dimensional surface, $S^{\mathrm{2D}}_{\varepsilon\varepsilon}(\gamma_1,\gamma_2)$.

It is assumed that the surface is isotropic, which allows the two-dimensional power spectral density to be inferred from any one-dimensional power spectral density. The following steps are performed [13]:

1. Perform the inverse Fourier transform on the spectral density of a rail $S_{\varepsilon_j\varepsilon_j}(\gamma)$ to obtain the auto-correlation function $R_{\varepsilon_j\varepsilon_j}(\chi)$.
2. If the surface is isotropic, the auto-correlation function of the surface will be equal to the auto-correlation function of a track, revolved about the origin axis. i.e. $R^{\mathrm{2D}}_{\varepsilon\varepsilon}(\chi_1,\chi_2) = R_{\varepsilon_j\varepsilon_j}(\sqrt{\chi_1^2+\chi_2^2})$.
3. Perform the two-dimensional Fourier transform on $R^{\mathrm{2D}}_{\varepsilon\varepsilon}(\chi_1,\chi_2)$ to obtain $S^{\mathrm{2D}}_{\varepsilon\varepsilon}(\gamma_1,\gamma_2)$.

For the power spectral density as defined earlier for a single track, an analytical expression for the autocorrelation function of each rail – and therefore for the autocorrelation function of the surface – can be obtained. Taking the inverse Fourier transform of the rectangular function yields the following:

$$R_{\varepsilon_j\varepsilon_j}(\chi) = 2S_0\gamma_{\max}\mathrm{sinc}(\gamma_{\max}\chi), \tag{35}$$

where $\mathrm{sinc}(x) = \sin(x)/x$, and so

$$R^{\mathrm{2D}}_{\varepsilon\varepsilon}(\chi_1,\chi_2) = 2S_0\gamma_{\max}\mathrm{sinc}\left(\gamma_{\max}\sqrt{\chi_1^2+\chi_2^2}\right). \tag{36}$$

Now the autocorrelation function is sampled over the desired range for χ_1,χ_2, and the double Fourier transform is performed to obtain a matrix of values for $S^{\mathrm{2D}}_{\varepsilon\varepsilon}(\gamma_1,\gamma_2)$. With the power spectral density of the surface determined, the cross spectral density can be calculated using the following equation [13]:

$$S_{\varepsilon_j\varepsilon_k}(\gamma_1) = \int_{-\infty}^{\infty} S^{\mathrm{2D}}_{\varepsilon\varepsilon}(\gamma_1,\gamma_2)\mathrm{e}^{\mathrm{i}\gamma_2\chi_{jk}}\,\mathrm{d}\gamma_2, \tag{37}$$

where $\chi_{jk} = (k-j)\chi_0 = (k-j)B/N_\varepsilon$ is the signed separation between rails j and k. Note that if $j=k$, the power spectral density (in this case, rectangular shaped) should be re-obtained, offering a means to verify the 2D power spectral density. For a surface of $\sigma_\varepsilon = 1\,\mu\mathrm{m}$ with a roller of radius R, the following 2D power spectral density shown in Figure 4 is obtained.

With the 2D spectral density of the surface obtained, the cross-spectral densities are determined using equation (37). For any given one-dimensional power spectral density, it can be shown that all cross-spectral densities are real for a surface of isotropic roughness: the two-dimensional power spectral density is rotationally symmetry, and therefore, for each value γ_1, is even in γ_2. In the integral of (37), the imaginary part $S^{\mathrm{2D}}_{\varepsilon\varepsilon}(\gamma_1,\gamma_2)\sin(\gamma_2\chi_{jk})$ is odd, and so cancels out in the infinite integral.

Using the above method, a series of cross spectral densities have been computed for a surface of rms

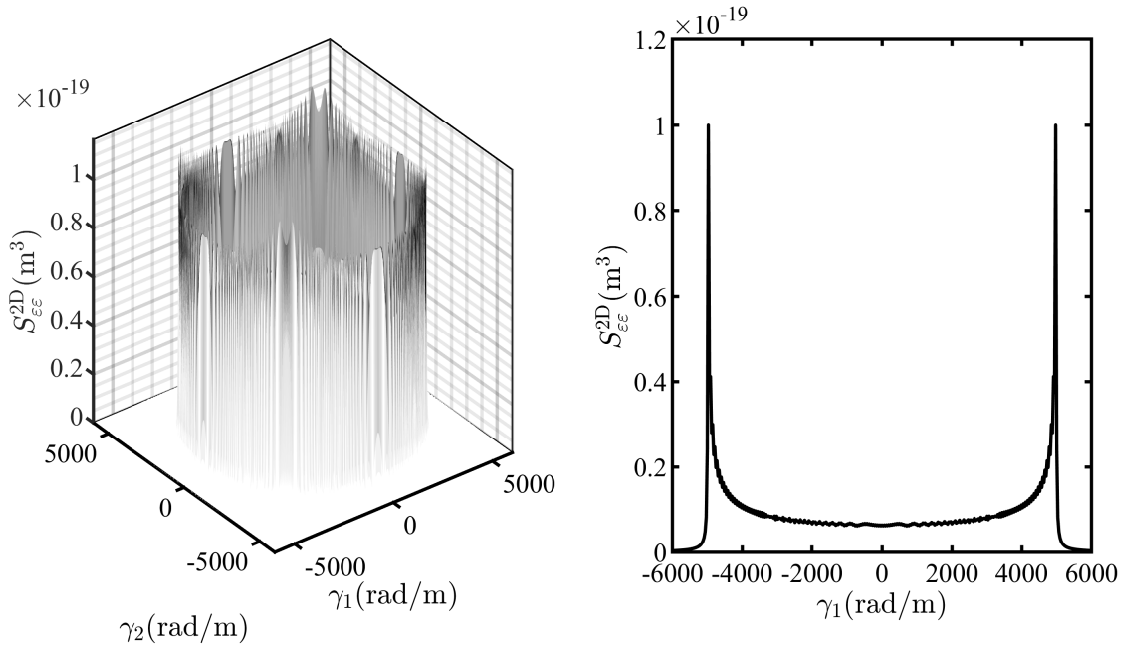

Figure 4. (left) The 2D spatial PSD of an isotropic surface corresponding to a rectangular PSD for a straight line along the surface, and (right) a cross-sectional view of the left.

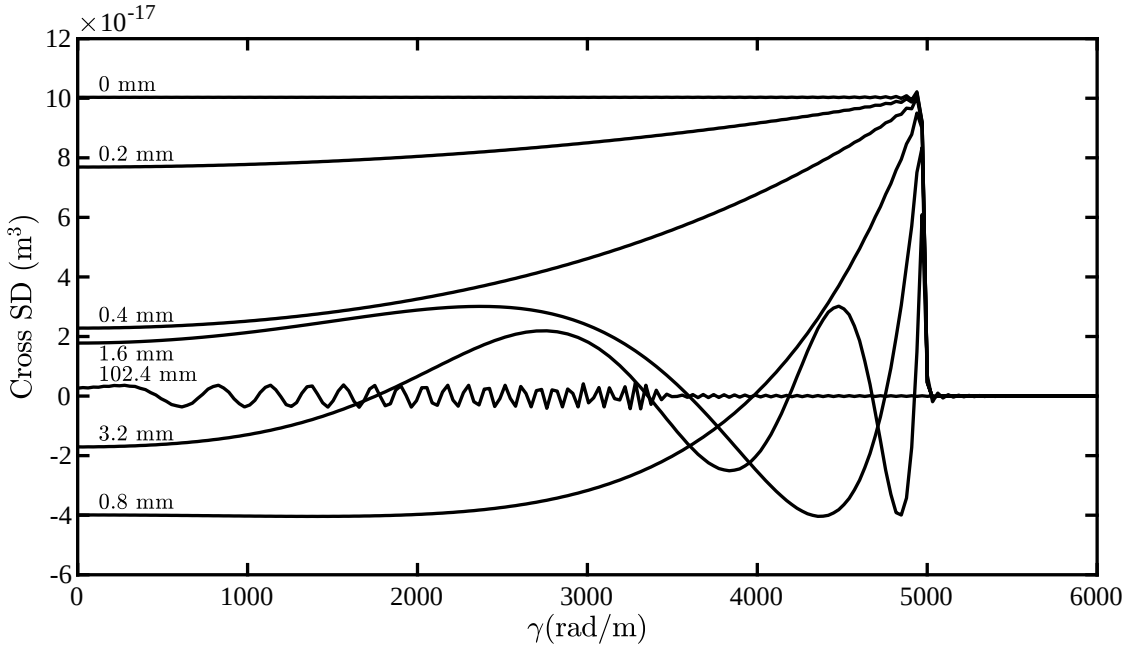

Figure 5. The cross spectral densities between parallel tracks for different separations for a surface of rms roughness $\sigma_\varepsilon = 1\,\mu\mathrm{m}$ and roller radius $R = 30\,\mathrm{mm}$.

roughness $\sigma_\varepsilon = 1\,\mu\mathrm{m}$ and roller radius $R = 30\,\mathrm{mm}$, as can be seen in Figure 5. For zero separation, the original rectangular function of the power spectral density of a single track is re-obtained: the input power spectral density was defined to have parameters (from Equations (32) and (33)) $\gamma_{\max} = 4980\,\mathrm{rad\,m^{-1}}$ and $S_0 = 1.00 \times 10^{-16}\,\mathrm{m}^3$. For small separation distances ($\sim 0.1\,\mathrm{mm}$) between tracks, the cross spectral density is approximately equal to the input power spectral density. For the region of the cross spectral density within $\gamma_{\max}$, the curve first touches zero when the separation is increased to $\chi_{jk} = \pi/\gamma_{\max} = 0.631\,\mathrm{mm}$. As the separation increases, the cross spectral density decreases for $\gamma < \gamma_{\max}$, but remains unchanged at $\gamma = \gamma_{\max}$.

As is, the cross spectral densities obtained are defined spatially for the surface roughness. To be used in the model, temporal cross spectral densities need to be obtained corresponding to the surface roughness at the point of contact with the roller. This transformation can be observed by extending Equation (34). Now that the cross-spectral densities can be output, the inputs into the model have been fully defined.

Table 2. The rms roller height, corresponding with Figure 6.

B	σ_{zz}
0 mm	$1.0003 \times 10^{-6}\,\mu$m
1 mm	$7.5196 \times 10^{-7}\,\mu$m
10 mm	$2.5116 \times 10^{-7}\,\mu$m
250 mm	$2.5110 \times 10^{-7}\,\mu$m

Table 3. The rms contact force, corresponding with Figure 7.

B	σ_{FF}
0 mm	3.8219 N
1 mm	3.3586 N
10 mm	1.2954 N
250 mm	0.9555 N

Results and discussion

The power spectral densities of the roller height and the contact force are obtained by inputting the calculated frequency response functions and the (cross) spectral densities of the parallel tracks of roughness into Equations (19) & (20). The parameters defined in Table 1 are used, a surface of rms roughness $1\,\mu$m and roller radius of $30\,$mm were selected, and $N_\varepsilon = 16$ tracks of roughness are used. The resulting power spectral densities are displayed in Figures 6 and 7. Note that this is performed for a number of values of B, which is the total width that the tracks of roughness cover, and can be thought as the effective length of the cylindrical roller. For the values $B = 0\,\text{mm}, 1\,\text{mm}, 10\,\text{mm}, 250\,\text{mm}$, the corresponding separation between neighbouring tracks are $B/N_\varepsilon = 0\,\text{mm}, 0.0625\,\text{mm}, 0.625\,\text{mm}, 15.625\,\text{mm}$ respectively. These various values, which includes the width of the reference bearing $250\,$mm, are investigated to see the impact of the separation between neighbouring tracks.

Note that since the maximum wavenumber of the input roughness power spectral density is $\gamma_{\text{max}} = 4980\,\text{rad}\,\text{m}^{-1}$, the maximum frequency of the power spectral density in time domain is $\omega_{\text{max}} = 1245\,\text{rad}\,\text{s}^{-1}$. This means that the frequency content at frequencies higher than this in the frequency response function have no role in the random vibration dynamics. As a result, in the range of interest, the frequency response function for this model including the beam-foundation system and that for a model excluding beam-foundation effects are very similar, which therefore suggests that the bulk deflection of the bearing race in a roller bearing has little influence on the response of the roller to surface roughness.

In Figure 6, the $B = 0$ case is very similar to the temporal power spectral density of a single track of roughness. For $B = 0$, it is expected that the results become the same as that for a single-track case: the separation between the 16 tracks are zero, so that all the tracks are exactly the same as one another, i.e. they are perfectly correlated. As a result, Equations (19) and (20) become the same as that for a single track. Note that the power spectral density is effectively the same as that for a track of roughness: the roller follows the surface roughness with relatively small contact deflections or bulk deflections of the beam, which is a result of the relatively high stiffnesses K, EI and k.

As B increases, the correlation between the neighbouring tracks decrease. In response, S_{zz} also decreases. Troughs along one track no longer necessarily correspond with troughs of other tracks, and so $z(t)$ deviates from zero to a lesser extent. Table 2 contains the rms values of $z(t)$ for each of the power spectral density curves, and indeed shows the corresponding decrease for increasing separation. The lowest possible value the rms can reduce to as a result of decreasing correlation is $1/\sqrt{N_\varepsilon}$ of the fully correlated value, provided the frequency response functions are the same for each track. Note how in the $B = 250\,$mm curve that sharp features are present that are characteristic of the oscillating curves in Figure 5, which may coincide with the separation between neighbouring tracks ($15.625\,$mm) being greater than the value required for the cross spectral density curve to first touch zero ($0.631\,$mm).

As for Figure 7, the same decrease in spectral density for increasing B is observed. Table 3 displays the calculated rms values of the contact force. From a single-track model, the rms contact force is estimated to be $3.8219\,$N. However, for a 16 track model with $B = 250\,$mm, this value drops to just above a quarter. The use of 16 tracks to cover a width of $B = 250\,$mm therefore suggests that a single-track model significantly overestimates the rms response.

The roller height and the contact force in the model then correspond to the radial position of a single bearing roller and the roller-race contact force in the actual bearing. Determining the power spectral density of the roller-race contact force provides stochastic information on the load cycle experienced between the roller and race due to the surface roughness, and this information could be used in assessing the impact of the loading cycle due to roughness on the fatigue life of the bearing.

Ideally, the addition of more tracks would allow results that are more representative of a cylinder of finite width, reducing more of the aforementioned overestimation. Eventually, we would expect the results to converge after a sufficiently large number of tracks. For the given number of tracks investigated (up to 16), no convergence was observed, and so more tracks are required. An estimation of the number of tracks required can be made by considering neighbouring tracks to be highly correlated. For instance, the case of $0.2\,$mm separation between neighbouring tracks (see Figure 5) suggests high correlation, and would require 1250 tracks. A disadvantage with the proposed method is that the computational complexity climbs rapidly, limiting the number of tracks that can be computed: convergence of results could not be obtained at this stage.

Conclusions

A model is developed to determine the response of a bearing roller to surface roughness, incorporating a beam-foundation system to model race deflections and using multiple tracks of roughness to better model the roughness of a surface.

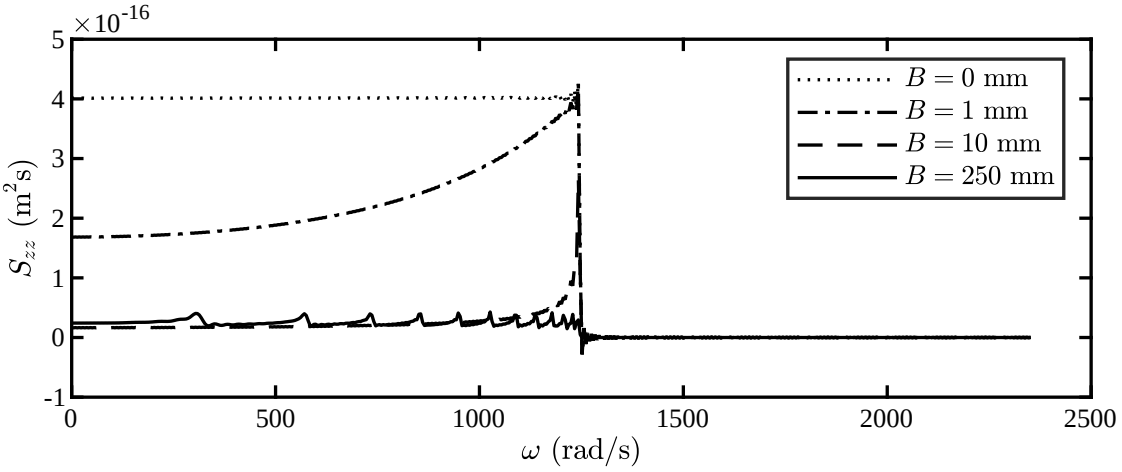

Figure 6. The power spectral density of the height of the roller, for a surface of rms roughness $\sigma_\varepsilon = 1\,\mu\mathrm{m}$ and roller radius $R = 30\,\mathrm{mm}$. Different lines correspond to different roller lengths.

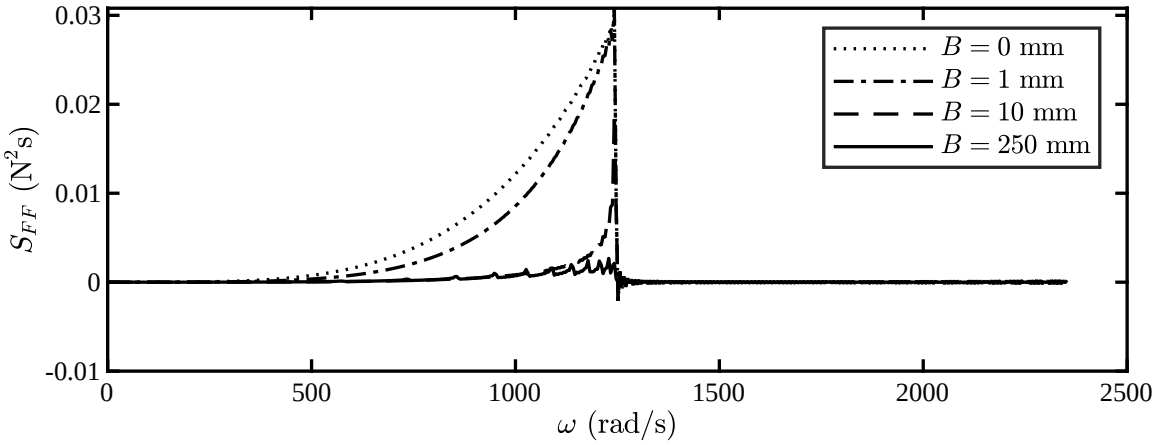

Figure 7. The power spectral density of the roller-race contact force, for a surface of rms roughness $\sigma_\varepsilon = 1\,\mu\mathrm{m}$ and roller radius $R = 30\,\mathrm{mm}$. Different lines correspond to different roller lengths.

A simplified model for surface roughness is used: white noise with a sharp cut-off frequency to account for the roller size.

For a surface of rms roughness $1\,\mu\mathrm{m}$ and roller radius $30\,\mathrm{mm}$, the contact stiffness and beam-foundation system stiffness has negligible impact on the response of the cylindrical roller. For the planet bearing considered, the influence of such stiffness would be negligible up to frequency contents around $20\,\mathrm{krad\,s^{-1}}$: such frequencies only arise for roughness below $0.06\,\mu\mathrm{m}$. Therefore, it can be concluded that this influence of stiffness can be neglected for wind turbine planet bearings.

At this stage, the curvature of the bearing race (as opposed to being straight like a beam) had been neglected. This was done initially for simplifying purposes. However, one way the results could be improved is by incorporating the radius of the race into an effective radius instead of using just the roller radius. That is,

$$\frac{1}{R_{ef}} = \frac{1}{R} + \frac{1}{R_{i/o}}. \tag{38}$$

where $R_{i/o}$ is the signed radius of the inner/outer race (negative for the concave outer race). In the future, the effect of curvature of the bearing race will be better incorporated into the model.

The use of multiple tracks of roughness can be used to model the roughness of a surface better than a single track model does. The power spectral densities of the roller height and contact force are overestimated in single track models. More tracks would reduce the overestimation, and the results would be expected to eventually converge. However, no such convergence was observed due to limitations of computation: the expense of the computation increased rapidly with the number of tracks.

At this stage, the results produced so far are obtained from numerical simulations of the model. This therefore begs the question of whether these results are indeed representative of real bearings. To answer this question, the authors intend to validate the model experimentally. That is, to compare an artificial signal generated by the model with a vibration sensor measured from an experimental rig using bearings with distributed faults.

Acknowledgements

This work was supported by the Engineering and Physical Sciences Research Council.

Declaration of conflicting interests

The Authors declare that there is no conflict of interest

References

1. Carroll J, McDonald A and McMillan D. Failure rate, repair time and unscheduled O&M cost analysis of offshore wind turbines. *Wind Energy* 2016; 19(6): 1107–1119.
2. Kotzalas MN and Doll GL. Tribological advancements for reliable wind turbine performance. *Philosophical Transactions of the Royal Society of London A: Mathematical, Physical and Engineering Sciences* 2010; 368(1929): 4829–4850.
3. Ruellan A, Ville F, Kleber X et al. Understanding white etching cracks in rolling element bearings: The effect of hydrogen charging on the formation mechanisms. *Proceedings of the Institution of Mechanical Engineers, Part J: Journal of Engineering Tribology* 2014; 228(11): 1252–1265.
4. Evans MH. An updated review: white etching cracks (WECs) and axial cracks in wind turbine gearbox bearings. *Materials Science and Technology* 2016; 32(11): 1133–1169.
5. Sawalhi N and Randall R. Simulating gear and bearing interactions in the presence of faults: Part II: Simulation of the vibrations produced by extended bearing faults. *Mechanical Systems and Signal Processing* 2008; 22: 1952–1966.
6. Dolenc B, Bokoski P and Juričić D. Distributed bearing fault diagnosis based on vibration analysis. *Mechanical Systems and Signal Processing* 2016; 66–67: 521–532.
7. Takabi J and Khonsari M. On the dynamic performance of roller bearings operating under low rotational speeds with consideration of surface roughness. *Tribology International* 2015; 86: 62–71.
8. Bogacz R and Kowalska Z. Computer simulation of the interaction between a wheel and a corrugated rail. *European Journal of Mechanics-A/Solids* 2001; 20(4): 673–684.
9. Dodds C and Robson J. The description of road surface roughness. *Journal of sound and vibration* 1973; 31(2): 175–183.
10. Nejad AR, Guo Y, Gao Z et al. Development of a 5 MW reference gearbox for offshore wind turbines. *Wind Energy* 2016; 19(6): 1089–1106.
11. Vesic AB. Beams on elastic subgrade and the Winklers hypothesis. In *Proceedings, 5th International Conference on Soil Mechanics and Foundation Engineering*, volume 1. pp. 845–850.
12. Fryba L. *Vibration of solids and structures under moving loads*. 1972.
13. Newland DE. *An introduction to random vibrations, spectral & wavelet analysis*. Courier Corporation, 2012.